A novel mycovirus evokes transcriptional rewiring in *Malassezia* and provokes host inflammation and an immunological response

Shelly Applen Clancey[1§], Fiorella Ruchti[2§], Salomé LeibundGut-Landmann[2*],

Joseph Heitman[1*], and Giuseppe Ianiri[1*$]

[1]Department of Molecular Genetics and Microbiology, Duke University Medical Center, 312 CARL Building, Box 3546 DUMC, Durham, NC, USA
[2]Section of Immunology, Vetsuisse Faculty, University of Zurich, Zurich, Switzerland

[$]Present address: Department of Agriculture, Environmental and Food Sciences, University of Molise, 86100, Campobasso, Italy

[§]These authors contributed equally to this work.

*Corresponding author:
Giuseppe Ianiri
Email: giuseppe.ianiri@unimol.it
Phone: +39 0874 404 662

Joseph Heitman
Email: heitm001@duke.edu
Phone: (919) 684-2824
Fax: (919) 684-2790

Salomé LeibundGut-Landmann
Email: salome.leibundgut-landmann@uzh.ch
Phone: +41-44-635-8721

Abstract

Mycoviruses infect fungi, and while most persist asymptomatically, there are examples of mycoviruses having both beneficial and detrimental effects on their host. Virus-infected *Saccharomyces* and *Ustilago* strains exhibit a killer phenotype conferring a growth advantage over uninfected strains, whereas hypovirus-infected *Cryphonectria parasitica* displays defects in growth, sporulation, and virulence. In this study we identify a dsRNA mycovirus in five *Malassezia* species. Sequence analysis reveals it to be a totivirus with two dsRNA segments: a larger 4.5 kb segment with genes involved in viral replication and maintenance, and a smaller 1.4 kb segment encoding a novel protein. Furthermore, RNA-seq of virus-infected versus virus-cured *Malassezia sympodialis* revealed an upregulation of dozens of ribosomal components in the cell, suggesting the virus subjects the cell to a large transcriptional burden. Given that *Malassezia* is the most abundant fungus on human skin, we assessed the impact of the mycovirus in a murine cutaneous infection model and found infection with virus-infected strains was associated with enhanced skin colonization and inflammatory response compared to virus-cured strains. Moreover, interferon-β expression was significantly upregulated in bone marrow-derived macrophages when challenged with virus-infected, compared to virus-cured *M. sympodialis*, suggesting that the presence of the virus can induce an immunological response. Although many recent studies have illuminated how widespread mycoviruses are, there are relatively fewer in depth studies about their impact on disease caused by the host fungus. We describe here a novel mycovirus in *Malassezia* and its possible implications in inflammatory disorders of the skin and possibly other tissues.

Importance

Malassezia species represent the most common fungal inhabitant of the mammalian skin microbiome, and are natural skin commensal flora. However, these fungi are also associated with a variety of clinical skin disorders. Recent studies have reported associations of

Malassezia with Crohn's disease and pancreatic cancer, further implicating this fungal genus in inflammatory and neoplastic disease states. Because *M. sympodialis* has lost genes involved in RNAi, we hypothesized *Malassezia* could harbor dsRNA mycoviruses. Indeed, we report here a novel mycovirus of the totivirus family in several *Malassezia* species, and characterized the MsMV1 mycovirus of *M. sympodialis*. We found conditions that lead to curing of the virus, and analyzed isogenic virus-infected/virus-cured strains to determine MsMV1 genetic and pathogenic impacts. MsMV1 induces a strong overexpression of transcription factors and ribosomal genes, while downregulating cellular metabolism. Moreover, MsMV1 leads to increased pathogenicity in a murine model, and induced a significantly higher level of interferon-β expression in cultured macrophages. This study sheds light on the mechanisms of pathogenicity of *Malassezia*, focusing on a previously unidentified novel mycovirus.

Introduction

Viruses are widely distributed in nature and are found in a variety of hosts, ranging from single-celled organisms to plants and mammals. The presence of mycoviruses, viruses that infect fungi, can be benign but are also associated with toxin secretion in yeast, hypovirulence in pathogenic plant fungi, and hypervirulence in dimorphic fungi (1-5). Mycoviruses are typically composed of double-stranded RNA (dsRNA) genomes, but positive-sense and negative-sense single-stranded RNA viruses, as well as circular ssDNA viruses have been reported to infect fungi (6). Overall, more than 10 different families of viruses have been isolated from fungal hosts (7). Despite similar genomic features shared between mycoviruses and human viruses from the same family, one clear difference between the two is the absence of cell-to-cell transmission proteins in mycoviruses. Therefore, mycoviruses typically lack an extracellular stage and are only transmitted during cell division, or by cell or hyphal fusion (8-10).

A well-known example of a mycovirus is the killer virus of *Saccharomyces cerevisiae*. This toxin-producing dsRNA virus was characterized in the 1970s (11), and found to have two dsRNA segments: a larger, 4.5 kb dsRNA, and a smaller, 1.5 kb satellite dsRNA. The large segment, called L-A, is required for viral replication and maintenance. The smaller segment, called M, encodes a preprotoxin, which is processed into a mature toxin by host enzymes and then secreted from the cell (12, 13). During the replication cycle of L-A, the single-stranded positive-strand ((+)ssRNA) is transcribed by the virally encoded replication machinery and released from the virion to serve two roles; 1) it is the mRNA template for translation of the Gag and Gag-Pol fusion protein, and 2) it is the template that is packaged into new viral particles where transcription reoccurs (13, 14). Yeast cells harboring both the L-A and M dsRNA segments display a growth advantage over strains lacking these components. When toxin-producing strains compete with wild-type strains, the virus-infected strains secrete the mature killer toxin, killing neighboring cells, whereas the toxin-producing cells remain unharmed (15). A similar fitness advantage is conferred by toxin-producing strains of *Ustilago maydis* (2).

In contrast to the killer viruses that provide virus-infected strains a growth advantage, the mycovirus that infects *Cryphonectria parasitica*, the causative agent of chestnut blight (which decimated the population of chestnut trees in the United States in the early 1900s by killing more than one billion trees) impairs growth of the fungus (16, 17). The growth defect of virus-infected strains results in reduced virulence, hence the name *Cryphonectria parasitica* hypovirus (CHV). Five different viral segments isolated from *C. parasitica* have been shown to confer a high level of hypovirulence, although the level of impact on fungal growth observed in the infected fungal strain appears to be virus strain-dependent (16, 18). A mycovirus infecting the filamentous fungus *Pseudogymnoascus destructans* has also been implicated in the epidemiology of white-nose syndrome, a lethal fungal infection in bats, as bats in North America have experienced 5 million deaths in the past decade, and all *P. destructans* isolates from bats in this region harbor a mycovirus (19). This is compared to European and Asian *P. destructans* isolates, which do not harbor the mycovirus, and the resident bat populations appear to be resistant to the endemic fungus.

RNAi is an important pathway conserved in many organisms and serves to regulate gene expression, suppress transposon movement, and maintain genome integrity. Additionally, a functional RNAi pathway has been shown to suppress mycovirus proliferation (20, 21). The biogenesis of small RNAs (sRNAs) originating from the infecting virus (termed virus-derived small interfering RNAs, or vsiRNAs) is analogous to that of endogenous sRNAs, requiring essential components such as dicer (*DCL*), argonaute (*AGO*), and RNA-dependent RNA polymerase (*RDP*) (22). It was previously thought that mycoviruses might only survive in species that lack a functional RNAi pathway as introduction of argonaute and dicer into yeast resulted in the elimination of the mycovirus (20). To this end, fungal species lacking canonical RNAi pathways have been good candidates in which to screen for mycoviruses. However, increased research on mycoviruses over the past decade has produced reports showing that mycoviruses have developed strategies to counteract the RNAi defense mechanisms that

suppress antiviral activity (5). In *Aspergillus nidulans*, infection of conidia with Virus 1816 suppresses inverted repeat transgene (IRT)-induced RNA silencing, and when the virus was cleared from ascospores, IRT silencing was restored (23). Other examples of mycovirus-induced RNAi suppression in *C. parasitica* and *Rosellinia necatrix* involve viral targeting of the RNAi machinery. In the case of *C. parasitica*, CHV1-EP713 encodes a papain-like protease (p29) that suppresses hairpin RNA-triggered silencing in the fungus (24). In *R. necatrix*, the mycoreovirus RnMyRV3 s10 gene encodes a product that appears to suppress RNA silencing by interfering with the dicing of dsRNA (25). Most recently, a novel partitivirus, TmPV1, was identified in *Talaromyces marneffei,* and is correlated with the downregulation of the *dcl*-1, *dcl*-2, and *qde*-2 RNAi genes in both virus-infected yeast and mycelia (4). Examples of virus-induced RNAi suppression spanning multiple classes of fungi is evidence that RNAi functions to control viral levels and that mycoviruses have evolved ways to counteract this regulation.

The genus *Malassezia* is a monophyletic group of lipophilic yeasts that colonize sebaceous skin sites and represent more than 90% of the skin mycobiome. Despite being a commensal yeast, *Malassezia* is associated with a number of common skin disorders, such as seborrheic dermatitis, atopic eczema, pityriasis versicolor, and also systemic infections (26). Recently, two landmark studies reported the association of *Malassezia* with gastrointestinal disorders such as Crohn's disease in a subset of patients with CARD9 mutations (which enhance sensitivity to fungal pathogen-associated molecular patterns [PAMPs]) and pancreatic cancer (27, 28), highlighting the importance of this understudied fungal genus as a crucial component of the human mycobiome. All *Malassezia* species lack the fatty acid synthase gene and thus are lipid-dependent, relying on exogenous fatty acids for growth. This feature makes *Malassezia* unique and fastidious to study under laboratory conditions, and as consequence relatively limited research has been done on the basic biology of this organism.

To date, 18 different species of *Malassezia* have been identified and sequence for 15 of these genomes is publicly available. Of these, the *M. sympodialis* ATCC42132 genome is the

most well annotated reference genome based on whole genome sequencing, RNA-seq, and proteomics (29, 30). As commensal inhabitants of the skin, *Malassezia* yeasts interact with the skin immune system, and specific T cells, as well as IgG and IgM antibodies, can be detected in healthy individuals, whereas specific IgE antibodies are prevalent in a large proportion of patients suffering from atopic eczema. A number of molecules with immunoglobulin E (IgE)-binding capabilities have been identified in extracts of *Malassezia* and have been named MalaS allergens. Ten allergens have been identified in *M. sympodialis*, and three in *M. furfur*. Eight of these allergens are conserved proteins that share high similarity with the corresponding mammalian homolog, suggesting that the induction of autoreactive T cells by *Malassezia* allergens could play a role in sustained inflammation (26, 31). Nevertheless, both the fungal and host factors contributing to the transition of *Malassezia* from commensal to pathogen are unknown and this is an active area of research.

Malassezia has a relatively small genome of 7.7 Mb, and due to its reduced size has lost nearly 800 genes compared to other sequenced Basidiomycota, including genes of the RNAi pathway (29). Given that *Malassezia* has lost the RNAi machinery, we hypothesized it could harbor mycoviruses and screened our collection of *Malassezia* strains for novel dsRNA viruses. Here, we report the discovery of a novel mycovirus from *M. sympodialis*, MsMV1. Following the screening of three dozen *M. sympodialis* isolates in our collection, we observed that this mycovirus is present in approximately 25% of the isolates. Fungal cells can be cured of the mycovirus upon exposure to high temperature or the antimicrobial agent biphenyl. RNA sequencing of infected and cured strain pairs revealed the complete genome of MsMV1 and illuminated a large shift in the cellular transcriptional profile comparing the congenic virus-infected and virus-cured strains. The presence of MsMV1 correlated with an increased ability to colonize and induce an inflammatory response in the skin, and we found that infection by MsMV1 resulted in increased production of interferon-β in cultured macrophages. These

findings reveal a novel mycovirus harbored by *Malassezia* with possible implications for interactions with the host in both the commensal and disease states.

Results

Identification and characterization of a novel mycovirus in *Malassezia*

Whole genome sequencing revealed that the *Malassezia* species have lost the genes required for a functional RNAi pathway (29); therefore, we hypothesized the fungus had the capacity to harbor mycoviruses. Following the screening of *M. sympodialis*, *M. pachydermatis,* and *M. furfur* laboratory freezer stocks, dsRNA species were detected in 11 of 36 *M. sympodialis* isolates (30.5%), one of three *M. pachydermatis* isolates (33.3%), and no *M. furfur* isolates. dsRNA species were also found in one of two *M. globosa* isolates, one *M. obtusa* isolate, and one *M. yamatoensis* isolate (Figure 1A, 1B, and Figure S1). For *M. sympodialis*, two dsRNA segments were visualized on an ethidium bromide-stained agarose gels, one at ~4.5 kb and another at ~1.4 kb. The sizes of these dsRNA segments are similar to those found in *S. cerevisiae* strains that produce killer toxins (1), suggesting the segments may correspond to a helper virus and a satellite RNA encoding a toxin precursor. *M. obtusa* and *M. yamatoensis* appear to only have the larger ~4.5 kb species as no dsRNA species of ~1.4 kb was detected. *M. globosa* also has a ~4.5 kb dsRNA species as well as two smaller species of ~500 bp and ~600 bp (Figure 1B).

In the present study we focused on the characterization of the mycovirus of *M. sympodialis* as a representative species of the *Malassezia* genus. To unveil the biological and physiological roles of the putative *Malassezia* mycovirus, a crucial first step was to define conditions that allow elimination (i.e. curing) of the mycovirus. In other fungi, mycoviruses can be cured by exposure to stressful conditions or certain drugs. In *S. cerevisiae*, exposure to the fungicide cycloheximide cures killer cells of the killer phenotype (32). This has varying rates of success in other organisms, such as *Aspergillus*, where a less than 50% success rate of mycovirus curing was observed after exposure to cycloheximide (33). In filamentous fungi, conidial isolation and hyphal tipping are more commonly used methods for curing (33), and polyethylene glycol was shown to cure *P. destructans* of PdPV-pa infection (19). To determine if

M. sympodialis could be cured of the dsRNA, the strains were passaged on modified Dixon's (mDixon) media and subjected to various stresses. We found that six passages on mDixon medium with no additives at high temperature (37°C) resulted in a complete loss of both dsRNA segments in four *M. sympodialis* virus-infected strains (Figure 1C, middle section). Following a single passage on mDixon medium with 10 µg/mL biphenyl, strains SEC555 and SEC557 derived from KS013 and KS016, respectively, lost both dsRNA species, while strains SEC554 and SEC558 (derived from KS012 and KS017, respectively) retained both dsRNA species (Figure 1C, right section). All dsRNA containing strains retained both segments when passaged on mDixon with no additives at 30°C (Figure 1C, left section).

To determine if the dsRNA moieties isolated from *M. sympodialis* are of viral origin, the dsRNA molecules of *M. sympodialis* were converted to cDNA and subjected to TA-cloning and Sanger sequencing. Clones of the large moiety were obtained from strain KS013, and from KS012 for the smaller one. Primer walking with Sanger sequencing revealed only partial insertions of the two into the cloning plasmid: a 1.3 kb region of the large ~4.5 kb segment, and a 374 bp portion of the ~1.4 kb segment. Blastx of the 1.3 kb sequence derived from the larger dsRNA revealed similarities with other mycoviruses deposited in GenBank, while a blastx search of 374 bp sequence derived from the smaller dsRNA found no hit (see later in the text for details). In parallel with the cDNA synthesis, cloning and sequencing, the congenic virus-infected and virus-cured strains KS012 and SEC494 of *M. sympodialis* were subjected to ribosomal RNA-depleted RNA sequencing. The rationale of the RNA-seq analysis was two-fold; first, allowing a more facile identification of the entire viral genome and second, elucidating possible transcriptomic changes evoked by the mycovirus in the host cells.

For the identification of the viral genome, adaptor-free RNAseq reads derived from *M. sympodialis* virus-infected and virus-cured isolates were assembled with Trinity. The resulting transcripts were searched using the sequences previously obtained through TA-cloning as a query, and two perfect hits (*E* value 0.0) were obtained following a blastn search against the

virus-infected strain KS012. Both hits are part of two larger independent contigs (DN8321 of 4613 bp, and DN4986 of 4601 bp; see File S1 legend for details) that subsequent analyses (described in detail below) reveal represent the entire viral genome. The two identified contigs are identical with the exception of a few nucleotides located at the sequence extremities and outside coding regions, likely being residual adaptor or assembly artifacts (File S1). Conversely, blastn analysis of the 1.3 kb viral TA-cloned sequence against the genome of the virus-cured isolate SEC494 found only a small 308 bp hit (*E* value 1e-143) that is part of the *M. sympodialis* ATCC42132 *MRP4* ortholog, which encodes a mitochondrial ribosomal protein of the small subunit (MSYG_4110, accession SHO79760). Combined with nucleic acid analysis based on agarose-ethidium bromide stained gels, this sequencing further supports that the dsRNA had been completely eliminated in the virus-cured strain.

Moreover, PCR analyses with primers designed to specific regions of the large and small dsRNA segments failed to produce amplicons on *M. sympodialis* KS012 genomic DNA, suggesting that the viral sequence is not integrated in the genome but is rather cytoplasmic. This finding is corroborated by *in silico* blast searches that failed to detect either large or small segment viral sequences in the *de novo* genome assembly of *M. sympodialis* KS012 (described below).

Using the ExPASy Translate web tool, the 4.6 kb segment was found to contain two open reading frames (ORFs), distinguished by a -1 ribosomal frameshift, a common feature of totiviruses (Figure 2A) (34). A BLASTp search of the ORF produced by a frame 1 translation revealed the RNA-dependent RNA polymerase gene (*RDP*) from *Scheffersomyces segobiensis* virus L (SsV L) with 52.69% homology. A BLASTp search of the ORF produced by a frame 2 translation identified the capsid protein from the same *S. segobiensis* virus, in this case with 53.87% homology (35). Phylogenetic analysis of the Rdp1 sequence obtained from RNA-seq grouped it with Rdp1 sequences from other mycoviruses of the totiviridae family (Figure 2B). Moreover, bidirectional blast analysis using the *S. segobiensis* SsV L virus genome as a query

against the *M. sympodialis* KS012 transcriptome assembly found the contigs DN8321 and DN4986 (File S1). These results strongly support that the large dsRNA segment isolated from *M. sympodialis* is a novel mycovirus and encodes proteins required for mycoviral replication and maintenance.

Similarly, the 374 bp query sequence from the smaller dsRNA segment identified via TA-cloning was subjected to a blastn search against the assembled transcriptomes of the virus-infected and virus-cured *M. sympodialis* strains KS012 and SEC494, respectively. Two highly significant hits (*E* value 3e -170 and 2e -166) were obtained only against the genome of the virus-infected strain KS012. The two hits are part of two independent contigs (DN7179 of 1546 bp and DN6052 of 1479 bp; see File S2 legend for details), consistent with the size of the small dsRNA segment based on agarose gel electrophoresis. These contigs are identical with the exception of a few nucleotides located at the sequence extremities and outside coding regions (File S2). Translation of this contig showed a single ORF (Figure 2C), which when used in a BLASTp search in NCBI returned only weak (≤29% homology, *E* value ≥1.6) hits to the 3' region of uncharacterized and hypothetical proteins in *Sporisorium reilianum* and *Streptomyces*, respectively; no significant hits were obtained from NCBI for the small segment.

To infer the function of this virally-encoded protein, the predicted amino acid sequence was subjected to domain prediction using Interpro Scan. A 305 amino acid non-cytoplasmic domain was identified at the C-terminal end of the protein and a short 19 amino acid signal peptide is predicted at the N-terminus (Figure 2D). Signal peptides are commonly present at the N-terminus of proteins that are destined for secretion. Signal peptides are composed of three regions: an N-region, an H-region, and a C-region. Typically, the N-region contains a stretch of positively charged amino acids, the H-region is the core of the signal peptide that contains a stretch of hydrophobic amino acids, and the C-region contains a stretch of amino acids that are recognized and cleaved by signal peptidases (36). The presence of this signal peptide, and the lack of homology to any protein in the NCBI database, suggests the ~1.5 kb dsRNA segment

from *M. sympodialis* encodes a previously unidentified, novel protein of unknown function that is likely secreted from the cell. Given the data supporting that these dsRNA segments represent a dsRNA virus in *M. sympodialis*, we termed this virus MsMV1 (*Malassezia sympodialis* mycovirus 1).

MsMV1 infection causes an upregulation of a large number of ribosomal genes

As described, total RNA from congenic virus-infected and virus-cured strain pairs KS012 and SEC494 was subjected to analysis of differentially expressed genes in the virus-infected strain compared to its cured counterpart. For RNA-seq analysis, three biological replicates of each sample were analyzed. RNA-seq reads of virus-infected and virus-cured strains KS012 and SEC494 were mapped against the reference *M. sympodialis* genome ATCC42132 using HiSat2. Transcript abundance was estimated through StringTie, and differentially expressed genes with a false discovery rate (FDR) < 0.05 and a $\log_2$-fold change +/- 1 were identified with EdgeR (37, 38).

The virus-infected strain displayed differential expression of 172 genes in comparison to the virus-cured strain, with 89 genes being upregulated ($\log_2$-fold change between 1 and 8.14) and 83 genes being downregulated ($\log_2$-fold change between -1 and -4.6) (Figure 3A). Among the proteins differentially upregulated, 50% are involved in ribosomal biogenesis and translation (Figure 3B). The remaining genes are involved in DNA replication and maintenance, transcription, stress responses, and other cellular metabolic processes. The most highly upregulated gene in the virus-infected strain, with a $\log_2$-fold change of 8.14, was MSYG_3592, encodes an uncharacterized mediator complex protein. The mediator complex is a transcriptional coactivator that interacts with transcription factors and RNA polymerase II, which transcribes all protein-coding and most non-coding RNA genes (39). The change in expression of this gene, combined with the upregulation of phosphorylation activity, ribosomal biogenesis, and cytoplasmic translation, indicates a large transcriptional shift in the virus-infected strain.

Downregulated genes included those involved in metabolic processes, oxidation-reduction processes, transmembrane transport, cell cycle and cell division, and many uncharacterized transcripts. In particular, the most downregulated gene that passed the FDR <0.05 threshold with a $\log_2$-fold change of -4.6 is an endoplasmic reticulum (ER) membrane protein, MSYG_1988, a gene whose predicted product is involved in the movement of substances across the ER membrane and/or protein synthesis. The second most downregulated gene is MSYG_0220 ($\log_2$-fold change = -4.1), which is an ortholog of *S. cerevisiae CDC39.* Cdc39 is a component of the Ccr4-Not1 complex that, in addition to its role as a global transcriptional regulator, regulates mRNA decay. These data suggest that elimination of aberrant mRNA transcripts may be inhibited in the virus-infected strain. Interestingly, we identified a gene (MSYG_3324) with the lowest $\log_2$-fold change (-11.88) that did not pass the statistically significant threshold of FDR <0.05. The gene MSYG_3324 gene encodes a hypothetical protein that has a guanine nucleotide exchange factor domain, leucine-rich repeats of the ribonuclease inhibitor (RI)-like subfamily, and an N-terminal Herpes BLLF1 superfamily domain, which consists of the BLLF1 viral late glycoprotein that is the most abundantly expressed glycoprotein in the viral envelope of the Herpes viruses. Strikingly, BLLF1 represents a major antigen responsible for production of neutralizing viral antibodies *in vivo* (40), and we speculate that it might be strongly downregulated by the MsMV1 mycovirus as a mechanism to dampen *M. sympodialis* antiviral defense systems. Overall our RNA-seq dataset is clearly indicative of a significant transcriptional rewiring of *M. sympodialis* in the presence of the dsRNA mycovirus MsMV1.

The three technical replicates of each strain produced highly similar expression profiles, which are distinct from one another (Figure 3C). The largest cluster of upregulated genes in the virus-infected strains included ribosomal components, and a gene network map shows the tight interaction of these ribosomal components (Figure 3D). The large, central cluster consists of

ribosomal proteins that are regulated by translation initiation factors Anb1 and Rpg1, and also Noc3, which bind ribosomal precursors to mediate their maturation and intranuclear transport.

One question that we sought to answer was whether the conditions employed to cure the virus changed the strain in any way other than virus elimination. We generated whole genome Illumina data and then performed genome-wide analyses and SNP calling of the *M. sympodialis* cured strain SEC494, comparing it to the virus-infected strain KS012. Only two nucleotide changes unique to the virus-cured isolate SEC494 were identified. These include mutations in the coding regions of *KAE1*, an ATPase, and *CRM1*, a karyopherin responsible for the transport of molecules between the cytoplasm and the nucleus (Table S1, File S3). Being as these mutations were only found in the virus-cured strain, they may be a consequence of the "curing treatment" and we predict their impact on fitness to be minimal given similar growth characteristics of the two strains (Table S1; File S3). Moreover, the assembled KS012 and SEC494 genomes are co-linear with the reference *M. sympodialis* genome ATCC42132, and no change in ploidy or aneuploidy was observed for any chromosome (Figure S2).

Virus-infected strains induce inflammation in a cutaneous murine model

In a recent study, Sparber and colleagues described a murine epicutaneous infection model that involves application of *Malassezia* to the mouse dorsal ear following mild tape stripping (41). Colonization of host tissue (fungal load) is determined by plating homogenized tissue onto agar plates and counting colony forming units; an increase in ear thickness is used as a measurement for skin inflammation. When mice were challenged with congenic virus-infected and virus-cured strains in this model, a more prominent ear thickening was observed in response to the virus-infected strains compared to their cured counterparts (Figure 4A, note statistical significance only for the KS012 and SEC494 virus-infected and virus-cured strain pairs). Moreover, for one of the two strain pairs tested, the virus-infected strain displayed increased colonization compared to their virus-cured counterpart by day 4 post-infection (Figure

4B). To determine if there was a difference in the immune response elicited by the virus-infected and virus-cured strains, we assessed the expression of interleukin-17 (IL-17), a key mediator of the host response against *Malassezia* on the skin (41). However, we could not detect any statistically significant differences in cytokine induction in response to virus-infected and virus-cured strains (Figure 4C), indicating that IL-17 expression was not regulated by the virus and not responsible for the observed differences in fungal load and skin thickness. We also assessed expression of IFN-β, a central player in antiviral immunity, but could not measure expression above the basal levels detected in the skin of naïve control animals (Figure 4C). The same was also true at earlier or later time points after infection (Figure S3).

Virus-infected strains induce interferon-β expression in bone marrow-derived macrophages in a TLR3-independent manner

Given its close relationship with the skin, *Malassezia* primarily interacts with keratinocytes and tissue-resident mononuclear phagocytes, including macrophages. Therefore, we assessed the interaction of *M. sympodialis* virus-infected and virus-cured strains with macrophages. Bone marrow-derived macrophages (BMDMs) are mature, differentiated bone marrow monocyte/macrophage progenitors that are suitable for host-pathogen interaction studies (42). Interferon-β (IFN-β) expression in BMDMs was measured by RT-qPCR following incubation with virus-infected and virus-cured *M. sympodialis* strains for 24 hours. The presence of MsMV1 induced significantly more IFN-β expression in BMDMs than virus-cured strains (Figure 5A).

In leishmaniasis, a parasitic disease caused by *Leishmania*, an elevated burden of *Leishmania* RNA virus-1 (LRV1) in the parasite is associated with parasite dissemination and increased disease severity (43, 44). Toll-like receptors (TLRs) are innate immune-recognition receptors known to play a role in viral infection, and TLR3, which recognizes and responds to dsRNA (45), was found to be required for the induction of pro-inflammatory factors and disease

exacerbation in leishmaniasis (43). Given the relationship between TLR3 and dsRNA recognition, TLR3 deficient BMDMs were incubated with the virus-infected and virus-cured *Malassezia* strains. In contrast to observations with LRV1, the increased production of IFN-β by MsMV1-infected strains was not dependent upon TLR3, as deletion of this gene in BMDMs did not result in a loss of IFN-β expression by the infected strains (Figure 5B).

BMDM viability and macrophage activation, as measured by $CD86^+$ surface expression and TNF expression, was also assessed (Figure S4A). No significant differences were found in BMDMs incubated with virus-infected and virus-cured *M. sympodialis* strains, and deletion of TLR3 did not change this result (Figure S3C). The seemingly enhanced induction of CD86 by the virus-cured strain SEC494 (Figure S4A) was not reproducible in independent repeat experiments, not paralleled by other readouts of macrophage activation, and not consistent with the results obtained with other virus-infected and virus-cured strain pairs. Therefore, it seems unlikely to be related to the absence of the virus.

Discussion

Mycoviruses are proving to be much more ubiquitous in nature than previously appreciated. Fungi harboring mycoviruses display a range of phenotypes, which in some cases can prove beneficial or detrimental for the host plant or animal. For instance, *C. parasitica* carries the CHV1 virus that causes reduced growth and pathogenicity of the fungus. Therefore, trees infected with virus-infected strains of *C. parasitica* display smaller cankers than trees infected with virus-free strains (16). Application of hypovirus-infected strains to infected cankers has proven to be an effective biocontrol agent as it halted the decimation of the chestnut tree in North America (17). Conversely, virus-infected *L. guyanesis* exacerbates leshmaniasis in mice and increases parasitemia, leading to the dissemination and metastasis of the parasite from the infection site (43).

Here, we describe the discovery of dsRNA mycoviruses in five *Malassezia* species: *M. sympodialis, M. pachydermatis, M. globosa, M. obtusa,* and *M. yamatoensis* (Figure 1A, 1B, and Supplemental Figure S1), and characterize in detail the MsMV1 virus from *M. sympodialis.* RNA-sequencing revealed the large dsRNA segment from *M. sympodialis* is of viral origin and contains two open reading frames that encode the Rdp1 and capsid proteins, which are translated by a -1 ribosomal frameshift, a hallmark feature of the Totiviridae virus family (Figure 2A)(34). In accord, phylogenetic analysis of the Rdp1 open reading frame groups most closely with other mycoviruses from the totiviridae family (Figure 2B). Using the small dsRNA segment sequence as a query, no significant matches were found in the NCBI database, suggesting the satellite virus is unique to this fungus and could serve a specialized role. Taken together, these data support the discovery of a novel mycovirus in the important skin fungus *M. sympodialis*. Further investigation will be required to characterize the presumptive mycoviruses in the other *Malassezia* species.

We find that exposure to high temperature (37°C) or to an antimicrobial agent (biphenyl) cures *M. sympodialis* of MsMV1 (Figure 1C). These are two conditions frequently encountered by fungi. Systemic human patient fungal isolates are exposed to high temperature during infection, and isolates from both patients and the environment are often purified on media containing antimicrobials to inhibit bacterial or filamentous fungal growth from the host or environment. It is possible these typical microbiological isolation methods may be inducing mycovirus curing during isolation. Taken together with the growing reports on their discovery of novel mycoviruses, mycoviruses may be much more abundant than currently appreciated. Not all of the *Malassezia* isolates analyzed in this study harbored a mycovirus, and this could reflect either natural diversity or curing during isolation. It is not clear why these two conditions cause virus curing. In the case of high temperature, this stressful condition may alter cellular physiology rendering the cell a less favorable host for the mycovirus. Viral replication and maintenance, while neutral at 30°C, could interfere with cellular processes required for survival

at 37°C. Moreover, high temperature is known to increase heat shock and misfolded proteins in the cell (46), and if full Hsp90 function is required for viral replication then the virus could be lost due to the overburdened Hsp90.

RNA-sequencing of virus-infected and virus-cured strains revealed major differences in the transcriptional profile between the two strains. Most notably is the upregulation of a large number of ribosomal components in the virus-infected strains. A similar result was found with the plant fungus *Sclerotinia sclerotiorum*, which harbors the SsHV2-L hypovirus, where rRNA metabolic processes and cellular component biogenesis were the classes of the most upregulated genes in virus-infected strains (47). Alternatively, the opposite has been observed in *S. cerevisiae*, where virus-infection is associated with the down-regulation of ribosome biogenesis and stress response, suggesting that in *S. cerevisiae*, virus-infected cells may be less stressed due to host protection systems for the killer virus (48).

Genes involved in oxidation-reduction processes are another category that was downregulated in the virus-infected strain. Denitrification, the biological process of converting nitrate to ammonia through reduction, which is then broken down into nitrogen, nitrous oxide, and nitric oxide (NO), is an important pathway in living organisms. NO is an important signaling molecule in bacteria and fungi. Furthermore, NO production is positively correlated with aflatoxin production in *A. nidulans*, where deletion of flavohemoglobin, a nitric oxide reductase, leads to reduced sterigmatocystin production and *aflR* expression (49). Flavohemoglobin, encoded for by the *YHB1* gene in *M. sympodialis*, does not appear to play a role in putative toxin producing strains as it is downregulated only 0.69-fold in MsMV1-infected strains. Recent work from Wisecaver and colleagues as well as our lab has identified that *Malassezia* acquired flavohemoglobin via a horizontal gene transfer event from *Corynebacterium* (49)(unpublished data). A likely explanation for the difference in the role of flavohemoglobin between *A. nidulans* is because the gene was not endogenous to *Malassezia* and rather acquired from an exogenous bacterial source, and therefore may not have been adapted to play a regulatory role

with the virus. The presence of the virus may be inducing the upregulation of transcriptional and translational machinery in order to synthesize components required for viral replication, maintenance, and persistence; how this signal is translated from the virus to the fungus is an interesting area for future research.

RNAi is a common antiviral defense system that operates in fungi to combat viral persistence in the cell. As expected, *C. parasitica* CHV1-infected cells exhibit an upregulation of silencing-related genes in an effort to reduce the viral burden or clear the virus. Alternatively, a different phenomenon occurs in *T. marneffei* TmPV1-infected cells where the virus can subsequently dampen expression of silencing-related genes and blunt the cellular RNAi defense mechanism (4, 50, 51). *M. sympodialis* has lost the canonical components of RNAi and hypothesize that the loss of RNAi may be contributing to mycovirus replication and persistence. Furthermore, we observed changes in genes related to regulating mRNA processing. One significantly downregulated gene is involved in mRNA decay, MSYG_0220 (*CDC39*). As described earlier, during the virus replication cycle, a ssRNA intermediate is formed prior to virion assembly (13) and is vulnerable to fungal defense mechanisms. Suppressing the expression of genes involved in eliminating anomalous mRNA transcripts could be a strategy for the virus to survive in the fungal cell. Interestingly, the RNA-seq analysis identified the downregulation of MSYG_03961 (*CPR3*) in virus-infected *M. sympodialis* cells. *CPR3* is a gene that encodes a mitochondrial cyclophilin (52) that could be linked to pathogenesis via established roles of mitochondria in basidiomycete pathogens (53).

Mycoviruses impact fungal virulence in different ways. Mycoviruses can be asymptomatic, whereas others induce either a hypo- or hyper-virulent state in the host fungus. We employed a recently developed murine model for *Malassezia* in which the fungus is applied onto the mouse ear following mild barrier disruption to replicate hallmarks of atopic dermatitis (41). We concluded that MsMV1 provides an enhanced virulence of *M. sympodialis* in this model because virus-infected strains displayed a modest advantage in the ability to colonize the

skin, and in the degree of fungus-induced inflammation, assessed as ear thickness, compared to their virus-cured counterparts (Figure 4A and 4B). Cultured macrophages also responded differently to virus-infected and virus-cured strains in which more IFN-β was produced from BMDMs incubated with virus-infected strains than virus-cured strains (Figure 5A). Furthermore, other parameters such as BMDM viability and BMDM activation were measured in parallel and no difference was detected between virus-infected and virus-cured strains (Figure S4A). Due to the role of IFN-β in the stimulation of antiviral and antiproliferative products (54), it is possible that the production of IFN-β may lead to enhanced clearing of virus-infected fungal cells from macrophages. TLR3 binds dsRNA in mammalian cells and was shown to play a critical role in disease exacerbation in leishmaniasis when the infecting *Leishmania* strain harbors a mycovirus (43, 44). In the case of *M. sympodialis*, we did not observe a requirement of TLR3 for IFN-β production in response to virus-infected strains (Figure 5B). Preliminary results also exclude cytosolic dsRNA recognition via a MAVS-dependent receptor to be involved in MsMV1 recognition (data not shown). Thus, we posit that dsRNA recognition by *Malassezia* may occur through an alternative virus recognition pathway yet to be elucidated that may recognize mycoviral dsRNA as a fungal pathogen-associated molecular pattern (PAMP).

In conclusion, we report for the first time evidence of mycoviruses infecting the fungal genus *Malassezia*. Although the target of the putative satellite toxin is unknown, it may induce an immune response in macrophages. Co-incubation of the virus-infected *M. sympodialis* with virus-cured *M. sympodialis* and bacterial species (*Escherichia coli, Corynebacterium* spp., and *Staphylococcus* spp.) failed to reveal antifungal or antibacterial properties of the virus-infected *M. sympodialis* strains. More research will be required to determine if this possible mycovirus toxin plays a role in common skin disorders caused by *Malassezia* by targeting the host, bacteria, or fungi of the skin microbiome.

Materials and methods

Strains

Malassezia sympodialis strains were stored at -80°C in 25% glycerol stocks and maintained on modified Dixon's (mDixon) medium at 30°C. mDixon media is composed of 3.6% malt extract, 1% mycological peptone, 1% desiccated ox bile, 1% Tween 60, 0.4% glycerol, and 2% agar for solid medium.

RNA extraction and dsRNA enrichment

Total RNA was extracted from *M. sympodialis* liquid cultures as follows. 5 mL liquid mDixon cultures were grown at 30°C until saturation, approximately 3-4 days. Cultures were pelleted at 3,000 rpm in a table top centrifuge for 3 minutes, washed with 5 mL dH_2O, and pellets were frozen at -80°C until lyophilization overnight. Following lyophilization, pellets were broken up with 3 mm glass beads and the RNA extraction was performed using TRIzol (ThermoFisher, 15596026) according to the manufacturer's instructions. RNA was resuspended in 50 µl diethyl pyrocarbonate (DEPC) water. RNA was treated with TURBO DNase (ThermoFisher, #AM2238) according to manufacturer's instructions, and resuspended in 50 µl DEPC water. ssRNA precipitation/dsRNA enrichment was done overnight at -20°C by combining 25 µl of DNase treated RNA, with 28 µl 8 M LiCl ([final]=2.8 M) and 27 µl DEPC water for a final volume of 80 µl. The mixture was centrifuged at 4°C for 10 minutes and the supernatant was recovered and transferred to a fresh eppendorf tube (the pellet can be saved and resuspended in 25 µl DEPC water as a ssRNA control). To the supernatant, 7.5 µl 3 M NaCl ([final]=0.1 M) and 187.5ul 100% ethanol ([final]=85%) was added and placed at -20°C for at least 1 hour. dsRNA was pelleted at 4°C for 15 minutes and resuspended in 25 µl DEPC water. To visualize dsRNA and ssRNA bands, 10 µl was electrophoresed on an 0.8% agarose gel stained with 5 µg/mL of ethidium bromide.

TA cloning of dsRNA segments

Large and small dsRNA segments were purified from *M. sympodialis* strains KS012, KS013, KS016, and KS017 as described above. Large and small dsRNA segments were excised from the agarose gel and purified via gel extraction using the QIAquick Gel Extraction Kit (Qiagen, 28704) 3' adapter sequences from the Illumina TruSeq Small RNA Library Preparation Kit (Illumina, RS-200) were ligated onto the dsRNA species by mixing together 1 µl of adapter with 1 µg dsRNA in a 6 µl reaction and heated at 70°C for 2 minutes. Following heating, tubes were immediately placed on ice. To the adapter reaction, 2 µl of HML ligation buffer, 1 µl RNasin, and 1 µl T4 RNA Ligase 2 (truncated) was added and mixed by pipetting. The solution was incubated for 1 hour at 28°C.

cDNA synthesis was achieved by combining 5 µl of adapter-ligated dsRNA with 1 µl RT primer and heated at 70°C for 2 minutes, then immediately placed on ice. Next, the adapter-ligated/RT primer mixture was used as template with the AffinityScript cDNA Synthesis Kit (Agilent, 600559) with the following reaction conditions: 25°C for 5 minutes, 55°C for 15 minutes, 95°C for 5 minutes. cDNA was PCR amplified using the RT primer, cloned into the pCR-Blunt vector using the Zero Blunt PCR Cloning Kit (Invitrogen, K270020), and transformed into *E. coli* with One Shot TOP10 Chemically Competent *E. coli* (Invitrogen, C404003). Plasmids were extracted from purified bacterial colonies and subjected to Sanger sequencing (Genewiz) using universal M13F and M13R primers.

RNA sequencing

5 mL liquid mDixon cultures were grown at 30°C for 3 days. Cells were pelleted at 3,000 rpm in a table top centrifuge for 3 minutes, washed with 5 mL dH_2O, and resuspended in 1 mL dH_2O. The 1 mL cell suspension was transferred to a bead beating tube with acid washed 425-600 µm beads. Cells were pelleted with beads in a microcentrifuge at 6,000 rpm for 2 minutes. The supernatant was removed and the cell pellet was flash frozen in liquid nitrogen. Frozen

566 bead/cell pellets were stored at -80°C until RNA extraction. To prepare RNA, bead/cells pellets
567 were thawed on ice and 1 mL TRIzol (ThermoFisher, 15596026) was added. Cells were bead
568 beated 10 times in 1 minute 'on', 1 minute 'rest' cycles. Following bead beating, 200 µl of
569 chloroform was added and the RNA extraction continued as described in the manufacturer's
570 instructions. Final RNA pellets were treated with TURBO DNase (ThermoFisher, AM2238)
571 according to manufacturer's instructions, and RNA was resuspended in 50 µl of nuclease free
572 water (Promega, P119A). Illumina 150 bp PE libraries were prepared using the TruSeq
573 Stranded Total RNA-seq Kit in combination with the Illumina Ribozero Yeast Kit. Library
574 preparation and RNA sequencing was performed at the Duke University Center for Genomic
575 and Computation Biology.

576 After sequencing, Illumina raw reads were trimmed with Trimmomatic to remove Illumina
577 adaptors (55). For the identification of the dsRNA mycovirus genome, one sequencing replicate
578 of both the virus-infected and virus-cured strains was assembled into a transcriptome using
579 Trinity (56), which was run on Galaxy (57). The generated transcriptome was searched using
580 the TA-cloned sequences derived from both the large and small dsRNA segments. *In silico*
581 functional characterization of the mycovirus sequences was performed through blast analyses
582 and InterPro scan (https://www.ebi.ac.uk/interpro/search/sequence/). For RNA-seq analysis, the
583 most recent *M. sympodialis* strain ATCC42132 genome assembly and annotation were used as
584 a reference (30). Illumina reads from three independent biological replicates were trimmed with
585 Trimmomatic as reported above, and cleaned reads were mapped to the *M. sympodialis*
586 reference genome using HiSat. Generated .bam files were used to run StringTie with the *M.*
587 *sympodialis* annotation as guide, and the –e option to provide the correct output for the
588 statistical analysis (37). Read count information for statistical analysis were extracted using a
589 provided python script (prepDE.py). EdgeR was used to determine the differentially expressed
590 genes (DEGs) in the *M. sympodialis* virus-infected strain KS012 compared to its cured
591 counterpart SEC494. StringTie and EdgeR were run on Galaxy (57). DEGs were considered

592 those with a FDR < 0.05 and with a $\log_2$-fold change ±1. Functional annotation of the DEGs was
593 performed using the Blast2GO pipeline, which includes the BLASTx against the NCBI non-
594 redundant protein database, gene ontology (GO) annotation and InterProScan (58). Heatmap
595 for the DEGs was generated using the web-based server heatmapper with the average linkage
596 for hierarchical clustering (http://www.heatmapper.ca/expression/), and gene network interaction
597 were determined using STRING (https://string-db.org/cgi/input.pl) with the *S. cerevisiae* protein
598 set as reference.

599 **Whole genome DNA sequencing and assembly**

600 25 mL liquid mDixon cultures of *M. sympodialis* KS012 and SEC494 were grown at 30°C
601 for 3 days. Cells were pelleted at 3,000 rpm in a table top centrifuge for 3 minutes, washed with
602 10 mL dH_2O, and cell pellets were frozen at -80°C. Cells pellets were lyophilized overnight,
603 pulverized using 3 mm glass beads, and subjected to genomic DNA extraction using the CTAB
604 method (59). Library preparation and 50 bp PE Illumina sequencing was performed at the Duke
605 University Center for Genomic and Computation Biology. Illumina reads for *M. sympodialis*
606 KS012 and SEC494 were assembled using SPAdes with default parameters (60). The de novo
607 genome assembly of *M. sympodialis* KS012 was used for blast searches using both large and
608 small dsRNA viral sequences.

609 Illumina reads of the *M. sympodialis* virus-infected strain KS012 and virus-cured
610 SEC494 were mapped to the *M. sympodialis* reference ATCC42132 using BWA (61), and the
611 resulting .sam file converted to .bam with samtools (62). Bam files were converted in .tdf format
612 using IGV, and the read coverage for *M. sympodialis* virus-infected strain KS012 and virus-
613 cured SEC494 visualized in the IGV browser using the *M. sympodialis* ATCC42132 as
614 reference. For variant analysis, the .bam files were generated as above and the *M. sympodialis*
615 reference ATCC42132 genome were used to run samtools mpileup; variant analysis was carried
616 out using the bcftools call option; the resulting .vcf file was merged with the *M. sympodialis*

annotation using the variant effector predictor software present on the EnsemblFungi database (https://fungi.ensembl.org/Malassezia_sympodialis_atcc_42132_gca_900149145/Info/Index).

Phylogenetic analysis

The MsMV1 Rdp1 was aligned with representative viral Rdp1 sequences found on NCBI using the Mega7 software. Phylogenies were built using 100 bootstrap values using the Maximum Likelihood method based on the Tamura-Nei model (63). Protein domains were predicted using NCBI Blastp and images were created using the MyDomain Image Creator from PROSITE on the ExPASy Bioinformatics resource portal.

Murine topical infection model

WT C57BL/6j mice were purchased by Janvier Elevage and maintained at the Laboratory Animal Science Center of University of Zurich, Zurich, Switzerland. Mice were used at 6-12 weeks in sex- and age-matched groups. Epicutaneous infection of the mouse ear skin was performed as described (41, 64). Briefly, *Malassezia* strains were grown for 3-4 days at 30°C, 180 rpm in liquid mDixon medium. Cells were washed in PBS and suspended in native olive oil at a density of 20 OD_{A600}/mL. 100 µl suspension (corresponding to 2 OD_{A600}) of yeast cells was applied topically onto the dorsal ear skin that was previously disrupted by mild tape stripping while mice were anaesthetized. Ear thickness was monitored prior and after infection using an Oditest S0247 0-5 mm measurement device (KROEPLIN) and the increase was calculated by subtracting the values measured prior to the experiments from those measured at the endpoint. For determining the fungal loads in the skin, tissue was transferred in water supplemented with 0.05% Nonidet P40 (AxonLab), homogenized and plated on modified Dixon agar and incubated at 30°C for 3-4 days.

Macrophage infection *in vitro*

Macrophages were generated from WT C57Bl/6j, *Tlr3*$^{-/-}$ (65) (Swiss Immunological Mouse Repository (SwImMR) hosted by the University of Zurich) bone marrow cells in the presence of 20% L929 conditioned R10* medium. After 6 days of culture, cells were detached using PBS/5% FCS/2.5 mM EDTA and seeded at a density of 10^5 cells/100 µl in 96-well tissue culture plates (for transcript analysis) and 10^6 cells/1 mL in 24-well plates (for FACS analysis). Cells were rested overnight and infected the next day with *Malassezia* at the indicated MOI for 16 hours (for FACS analysis) or for 24 hours (for transcript analysis). PolyI:C (50 µg/mL) was included as a control.

Flow cytometry

Macrophages were gently detached by using cell scrapers and stained with antibodies directed against CD11b (clone M1/70), F4/80 (clone BM8), CD86 (clone GL-1), and MHC-II (clone M5/114.15.2) in PBS supplemented with 1% FCS, 5 mM EDTA and 0.02% NaN_3. LIVE/DEAD Near IR stain (Life Technologies) was used for exclusion of dead cells. Cells were acquired on a FACS Cytoflex (Beckman Coulter) and the data were analyzed with FlowJo software (FlowJo LLC). The gating of the flow cytometric data was performed according to the guidelines for the use of flow cytometry and cell sorting in immunological studies (66), including pre-gating on viable and single cells for analysis.

RNA extraction and quantitative RT-PCR

Isolation of total RNA from ear skin and from BMDM cultures was carried out according to standard protocols using TRI Reagent (Sigma Aldrich). cDNA was generated by RevertAid reverse transcriptase (ThermoFisher). Quantitative PCR was performed using SYBR Green (Roche) and a QuantStudio 7 Flex (Life Technologies) instrument. The primers used for qPCR were as follows: *Il17a* forward 5'-GCTCCAGAAGGCCCTCAGA-3', reverse 5'-AGCTTTCCCTCCGCATTGA-3' (67); *Tnf* forward 5'-CATCTTCTCAAAATTCGAGTGACAA-3',

reverse 5'-TGGGAGTAGACAAGGTACAACCC-3' (68); *Ifnb* forward 5'-AACCTCACCTACAGGGC-3', reverse 5'-CATTCTGGAGCATCTCTTGG-3' (43); *Actb* forward 5--CCCTGAAGTACCCCATTGAAC-3', reverse 5'-CTTTTCACGGTTGGCCTTAG-3'. All RT-qPCR assays were performed in duplicate and the relative expression (rel. expr.) of each gene was determined after normalization to *Actb* transcript levels.

Data availability

Both sequencing reads for *M. sympodialis* virus-infected strain KS012 and *M. sympodialis* virus-cured strain SEC494 are available in the NCBI SRA database (BioProject PRJNA593722). The mycovirus genome has been deposited in GenBank under accession number MN812428.

Acknowledgements

We thank Marco A. Coelho for performing the genomic assemblies of the virus-infected and virus-cured *M. sympodialis* KS012 and SEC494 strains. This work was supported by NIH/NIAID R37 award AI39115-21 and R01 award AI50113-15 awarded to JH and by SNSF grant 310030_189255 awarded to SLL. JH is a Co-Director and Fellow of the CIFAR program Fungal Kingdom: Threats & Opportunities. We thank Blake Billmyre and other members of the Heitman lab, as well as Florian Sparber, Amanda McLeod, and Jessica Shannon for helpful discussions and comments on the manuscript.

References

1. Bevan EA, Herring AJ, Mitchell DJ. 1973. Preliminary characterization of two species of dsRNA in yeast and their relationship to the “killer” character. *Nature* 245:81-86.
2. Park C-M, Banerjee N, Koltin Y, Bruenn JA. 1996. The *Ustilago maydis* virally encoded KP1 killer toxin. *Molecular Microbiology* 20:957-963.
3. Wu M, Jin F, Zhang J, Yang L, Jiang D, Li G. 2012. Characterization of a novel bipartite double-stranded RNA mycovirus conferring hypovirulence in the phytopathogenic fungus *Botrytis porri*. *Journal of Virology* 86:6605-6619.
4. Lau SKP, Lo GCS, Chow FWN, Fan RYY, Cai JJ, Yuen K-Y, Woo PCY. 2018. Novel partitivirus enhances virulence of and causes aberrant gene expression in *Talaromyces marneffei*. *mBio* 9:e00947-18.
5. Son M, Yu J, Kim K-H. 2015. Five questions about mycoviruses. *PLoS Pathogens* 11:e1005172.
6. Ghabrial SA, Castón JR, Jiang D, Nibert ML, Suzuki N. 2015. 50-plus years of fungal viruses. *Virology* 479-480:356-368.
7. King AMQ, Adams MJ, Carstens EB, Lefkowitz EJ. 2012. Part II. The Viruses, p 21-36, *Virus Taxonomy* doi:https://doi.org/10.1016/B978-0-12-384684-6.00115-4. Elsevier, San Diego.
8. Ghabrial SA, Suzuki N. 2009. Viruses of plant pathogenic fungi. *Annual Review of Phytopathology* 47:353-384.
9. Fink GR, Styles CA. 1972. Curing of a killer factor in *Saccharomyces cerevisiae*. *PNAS* 69:2846-49.
10. Bevan EA, Somers JM. 2009. Somatic segregation of the killer (k) and neutral (n) cytoplasmic genetic determinants in yeast. *Genetical Research* 14:71-77.
11. Herring AJ, Bevan EA. 1974. Virus-like particles associated with the double-stranded RNA species found in killer and sensitive strains of the yeast *Saccharomyces cerevisiae*. *Journal of General Virology* 22:387-394.
12. Bostian KA, Elliott Q, Bussey H, Bum V, Smith AI, Tipper DJ. 1984. Sequence of the preprotoxin dsRNA gene of type I killer yeast: multiple processing events produce a two-component toxin. *Cell* 36:741-751.
13. Schmitt MJ, Breinig F. 2006. Yeast viral killer toxins: lethality and self-protection. *Nature Reviews Microbiology* 4:212-221.
14. Wickner RB. 1996. Double-stranded RNA viruses of *Saccharomyces cerevisiae*. *Microbiological reviews* 60:250-265.
15. Somers JM, Bevan EA. 2009. The inheritance of the killer character in yeast. *Genetical Research* 13:71-83.
16. Chen B, Nuss DL. 1999. Infectious cDNA clone of hypovirus CHV1-Euro7: a comparative virology approach to investigate virus-mediated hypovirulence of the chestnut blight fungus *Cryphonectria parasitica*. *Journal of Virology* 73:985-992.
17. Rigling D, Prospero S. 2018. *Cryphonectria parasitica*, the causal agent of chestnut blight: invasion history, population biology and disease control. *Molecular Plant Pathology* 19:7-20.
18. Hillman BI, Suzuki N. 2004. Viruses of the chestnut blight fungus, *Cryphonectria parasitica*, p 423-472, Advances in Virus Research, vol 63. Academic Press.
19. Thapa V, Turner GG, Hafenstein S, Overton BE, Vanderwolf KJ, Roossinck MJ. 2016. Using a novel partitivirus in *Pseudogymnoascus destructans* to understand the epidemiology of white-nose syndrome. *PLoS Pathogens* 12:e1006076.
20. Drinnenberg IA, Fink GR, Bartel DP. 2011. Compatibility with killer explains the rise of RNAi-deficient fungi. *Science* 333:1592-1592.

21. Segers GC, Zhang X, Deng F, Sun Q, Nuss DL. 2007. Evidence that RNA silencing functions as an antiviral defense mechanism in fungi. *PNAS* 104:12902-12906.
22. Deleris A, Gallego-Bartolome J, Bao J, Kasschau KD, Carrington JC, Voinnet O. 2006. Hierarchical action and inhibition of plant dicer-like proteins in antiviral defense. *Science* 313:68-71.
23. Hammond TM, Andrewski MD, Roossinck MJ, Keller NP. 2008. *Aspergillus* mycoviruses are targets and suppressors of RNA silencing. *Eukaryotic Cell* 7:350-357.
24. Segers GC, van Wezel R, Zhang X, Hong Y, Nuss DL. 2006. Hypovirus papain-like protease p29 suppresses RNA silencing in the natural fungal host and in a heterologous plant system. *Eukaryotic Cell* 5:896-904.
25. Yaegashi H, Yoshikawa N, Ito T, Kanematsu S. 2013. A mycoreovirus suppresses RNA silencing in the white root rot fungus, *Rosellinia necatrix*. *Virology* 444:409-416.
26. Gaitanis G, Magiatis P, Hantschke M, Bassukas ID, Velegraki A. 2012. The *Malassezia* genus in skin and systemic diseases. *Clinical Microbiology Reviews* 25:106-141.
27. Limon JJ, Tang J, Li D, Wolf AJ, Michelsen KS, Funari V, Gargus M, Nguyen C, Sharma P, Maymi VI, Iliev ID, Skalski JH, Brown J, Landers C, Borneman J, Braun J, Targan SR, McGovern DPB, Underhill DM. 2019. *Malassezia* is associated with Crohn's disease and exacerbates colitis in mouse models. *Cell Host & Microbe* 25:377-388.
28. Aykut B, Pushalkar S, Chen R, Li Q, Abengozar R, Kim JI, Shadaloey SA, Wu D, Preiss P, Verma N, Guo Y, Saxena A, Vardhan M, Diskin B, Wang W, Leinwand J, Kurz E, Kochen Rossi JA, Hundeyin M, Zambrinis C, Li X, Saxena D, Miller G. 2019. The fungal mycobiome promotes pancreatic oncogenesis via activation of MBL. *Nature* 574:264-267.
29. Wu G, Zhao H, Li C, Rajapakse MP, Wong WC, Xu J, Saunders CW, Reeder NL, Reilman RA, Scheynius A, Sun S, Billmyre BR, Li W, Averette AF, Mieczkowski P, Heitman J, Theelen B, Schröder MS, De Sessions PF, Butler G, Maurer-Stroh S, Boekhout T, Nagarajan N, Dawson TL, Jr. 2015. Genus-wide comparative genomics of *Malassezia* delineates its phylogeny, physiology, and niche adaptation on human skin. *PLoS Genetics* 11:e1005614.
30. Zhu Y, Engström PG, Tellgren-Roth C, Baudo CD, Kennell JC, Sun S, Billmyre RB, Schröder MS, Andersson A, Holm T, Sigurgeirsson B, Wu G, Sankaranarayanan SR, Siddharthan R, Sanyal K, Lundeberg J, Nystedt B, Boekhout T, Dawson TL, Jr., Heitman J, Scheynius A, Lehtiö J. 2017. Proteogenomics produces comprehensive and highly accurate protein-coding gene annotation in a complete genome assembly of *Malassezia sympodialis*. *Nucleic Acids Research* 45:2629-2643.
31. Glatz M, Bosshard PP, Hoetzenecker W, Schmid-Grendelmeier P. 2015. The role of *Malassezia* spp. in atopic dermatitis. *Journal of Clinical Medicine* 4:1217-1228.
32. Fink GR, Styles CA. 1972. Curing of a killer factor in *Saccharomyces cerevisiae*. *Proceedings of the National Academy of Sciences* 69:2846.
33. Kotta-Loizou I, Coutts RHA. 2017. Mycoviruses in *Aspergilli*: a comprehensive review. *Frontiers In Microbiology* 8:1699-1699.
34. Dinman JD, Icho T, Wickner RB. 1991. A -1 ribosomal frameshift in a double-stranded RNA virus of yeast forms a gag-pol fusion protein. *PNAS* 88:174-178.
35. Taylor DJ, Ballinger MJ, Bowman SM, Bruenn JA. 2013. Virus-host co-evolution under a modified nuclear genetic code. *PeerJ* 1:e50.
36. Käll L, Krogh A, Sonnhammer ELL. 2004. A combined transmembrane topology and signal peptide prediction method. *Journal of Molecular Biology* 338:1027-1036.
37. Pertea M, Kim D, Pertea GM, Leek JT, Salzberg SL. 2016. Transcript-level expression analysis of RNA-seq experiments with HISAT, StringTie, and Ballgown. *Nature Protocols* 11:1650-1667.

38. Robinson MD, McCarthy DJ, Smyth GK. 2010. edgeR: a Bioconductor package for differential expression analysis of digital gene expression data. *Bioinformatics* 26:139-140.
39. Allen BL, Taatjes DJ. 2015. The Mediator complex: a central integrator of transcription. *Nature Reviews* 16:155-166.
40. Janz A, Oezel M, Kurzeder C, Mautner J, Pich D, Kost M, Hammerschmidt W, Delecluse HJ. 2000. Infectious Epstein-Barr virus lacking major glycoprotein BLLF1 (gp350/220) demonstrates the existence of additional viral ligands. *Journal of Virology* 74:10142-10152.
41. Sparber F, De Gregorio C, Steckholzer S, Ferreira FM, Dolowschiak T, Ruchti F, Kirchner FR, Mertens S, Prinz I, Joller N, Buch T, Glatz M, Sallusto F, LeibundGut-Landmann S. 2019. The skin commensal yeast *Malassezia* triggers a type 17 response that coordinates anti-fungal immunity and exacerbates skin inflammation. *Cell Host & Microbe* 25:389-403.
42. Weischenfeldt J, Porse B. Bone marrow-derived macrophages (BMM): isolation and applications. *Cold Spring Harbor Protocols* 2008; doi:10.1101/pdb.prot5080.
43. Ives A, Ronet C, Prevel F, Ruzzante G, Fuertes-Marraco S, Schutz F, Zangger H, Revaz-Breton M, Lye L-F, Hickerson SM, Beverley SM, Acha-Orbea H, Launois P, Fasel N, Masina S. 2011. *Leishmania* RNA virus controls the severity of mucocutaneous leishmaniasis. *Science* 331:775-778.
44. de Carvalho RVH, Lima-Junior DS, da Silva MVG, Dilucca M, Rodrigues TS, Horta CV, Silva ALN, da Silva PF, Frantz FG, Lorenzon LB, Souza MM, Almeida F, Cantanhêde LM, Ferreira RdGM, Cruz AK, Zamboni DS. 2019. Leishmania RNA virus exacerbates Leishmaniasis by subverting innate immunity via TLR3-mediated NLRP3 inflammasome inhibition. *Nature Communications* 10:5273.
45. Alexopoulou L, Holt AC, Medzhitov R, Flavell RA. 2001. Recognition of double-stranded RNA and activation of NF-κB by Toll-like receptor 3. *Nature* 413:732-738.
46. Parsell DA, Lindquist S. 1993. The function of heat-shock proteins in stress tolerance: degradation and reactivation of damaged proteins. *Annual Review of Genetics* 27:437-496.
47. Lee Marzano S-Y, Neupane A, Domier L. 2018. Transcriptional and small RNA responses of the white mold fungus *Sclerotinia sclerotiorum* to infection by a virulence-attenuating hypovirus. *Viruses* 10:713.
48. Lukša J, Ravoitytė B, Konovalovas A, Aitmanaitė L, Butenko A, Yurchenko V, Serva S, Servienė E. 2017. Different metabolic pathways are involved in response of *Saccharomyces cerevisiae* to L-A and M viruses. *Toxins* 9:233.
49. Baidya S, Cary JW, Grayburn WS, Calvo AM. 2011. Role of nitric oxide and flavohemoglobin homolog genes in *Aspergillus nidulans* sexual development and mycotoxin production. *Applied and Environmental Microbiology* 77:5524-5528.
50. Zhang X, Segers GC, Sun Q, Deng F, Nuss DL. 2008. Characterization of hypovirus-derived small RNAs generated in the chestnut blight fungus by an inducible *DCL-2*-dependent pathway. *Journal of Virology* 82:2613-2619.
51. Sun Q, Choi GH, Nuss DL. 2009. A single Argonaute gene is required for induction of RNA silencing antiviral defense and promotes viral RNA recombination. *PNAS* 106:17927-17932.
52. Davis ES, Becker A, Heitman J, Hall MN, Brennan MB. 1992. A yeast cyclophilin gene essential for lactate metabolism at high temperature. *PNAS* 89:11169-11173.
53. Ma H, Hagen F, Stekel DJ, Johnston SA, Sionov E, Falk R, Polacheck I, Boekhout T, May RC. 2009. The fatal fungal outbreak on Vancouver Island is characterized by enhanced intracellular parasitism driven by mitochondrial regulation. *PNAS* 106:12980-12985.

54. Bekisz J, Sato Y, Johnson C, Husain SR, Puri RK, Zoon KC. 2013. Immunomodulatory effects of interferons in malignancies. *Journal of Interferon & Cytokine Research* 33:154-161.
55. Bolger AM, Lohse M, Usadel B. 2014. Trimmomatic: a flexible trimmer for Illumina sequence data. *Bioinformatics* 30:2114-2120.
56. Haas BJ, Papanicolaou A, Yassour M, Grabherr M, Blood PD, Bowden J, Couger MB, Eccles D, Li B, Lieber M, MacManes MD, Ott M, Orvis J, Pochet N, Strozzi F, Weeks N, Westerman R, William T, Dewey CN, Henschel R, LeDuc RD, Friedman N, Regev A. 2013. *De novo* transcript sequence reconstruction from RNA-seq using the Trinity platform for reference generation and analysis. *Nature Protocols* 8:1494-1512.
57. Afgan E, Baker D, Batut B, van den Beek M, Bouvier D, Cech M, Chilton J, Clements D, Coraor N, Grüning BA, Guerler A, Hillman-Jackson J, Hiltemann S, Jalili V, Rasche H, Soranzo N, Goecks J, Taylor J, Nekrutenko A, Blankenberg D. 2018. The Galaxy platform for accessible, reproducible, and collaborative biomedical analyses: 2018 update. *Nucleic Acids Research* 46:W537-W544.
58. Conesa A, Götz S, García-Gómez JM, Terol J, Talón M, Robles M. 2005. Blast2GO: a universal tool for annotation, visualization, and analysis in functional genomics research. *Bioinformatics* 21:3674-3676.
59. Pitkin JW, Panaccione DG, Walton JD. 1996. A putative cyclic peptide efflux pump encoded by the TOXA gene of the plant-pathogenic fungus *Cochliobolus carbonum*. *Microbiology* 142:1557-1565.
60. Bankevich A, Nurk S, Antipov D, Gurevich AA, Dvorkin M, Kulikov AS, Lesin VM, Nikolenko SI, Pham S, Prjibelski AD, Pyshkin AV, Sirotkin AV, Vyahhi N, Tesler G, Alekseyev MA, Pevzner PA. 2012. SPAdes: a new genome assembly algorithm and its applications to single-cell sequencing. *Journal of Computational Biology* 19:455-477.
61. Li H, Durbin R. 2010. Fast and accurate long-read alignment with Burrows-Wheeler transform. *Bioinformatics* 26:589-595.
62. Li H, Handsaker B, Wysoker A, Fennell T, Ruan J, Homer N, Marth G, Abecasis G, Durbin R, Genome Project Data Processing S. 2009. The sequence alignment/map format and SAMtools. *Bioinformatics* 25:2078-2079.
63. Tamura K, Nei M. 1993. Estimation of the number of nucleotide substitutions in the control region of mitochondrial DNA in humans and chimpanzees. *Molecular Biology and Evolution* 10:512-526.
64. Sparber F, LeibundGut-Landmann S. 2019. Infecting mice with *Malassezia* spp. to study the fungus-host interaction. *Journal of Visualized Experiments* doi:doi:10.3791/60175:e60175.
65. Honda K, Sakaguchi S, Nakajima C, Watanabe A, Yanai H, Matsumoto M, Ohteki T, Kaisho T, Takaoka A, Akira S, Seya T, Taniguchi T. 2003. Selective contribution of IFN-alpha/beta signaling to the maturation of dendritic cells induced by double-stranded RNA or viral infection. *PNAS* 100:10872-10877.
66. Cossarizza A, al e. 2019. Guidelines for the use of flow cytometry and cell sorting in immunological studies (second edition). *European Journal of Immunology* 49:1457-1973.
67. Overbergh L, Giulietti A, Valckx D, Decallonne R, Bouillon R, Mathieu C. 2003. The use of real-time reverse transcriptase PCR for the quantification of cytokine gene expression. *Journal of Biomolecular Techniques* 14:33-43.
68. Schönherr FA, Sparber F, Kirchner FR, Guiducci E, Trautwein-Weidner K, Gladiator A, Sertour N, Hetzel U, Le GTT, Pavelka N, d'Enfert C, Bougnoux ME, Corti CF, LeibundGut-Landmann S. 2017. The intraspecies diversity of *C. albicans* triggers qualitatively and temporally distinct host responses that determine the balance between commensalism and pathogenicity. *Mucosal Immunology* 10:1335-1350.

Figure legends

Figure 1. *Malassezia* species harbor dsRNA segments. A) dsRNA from representative *M. sympodialis* strains. B) dsRNA from additional *Malassezia* species. Strain names can be found in Table 1. C) dsRNA from *M. sympodialis* strains passaged at 30°C, 37°C, and on mDixon media containing 10 µg/mL biphenyl. dsRNA (upper panel) and ssRNA (lower panel) were visualized by electrophoresis in 0.8% agarose gels with 0.5 µg/mL ethidium bromide.

Figure 2. dsRNA segments code for viral protein products. A) Representative region of the large dsRNA segment illustrating the two open reading frames for the capsid and Rdp1 and the site of the -1 ribosomal frameshift. Stop codon for capsid highlighted in red. Start codon for Rdp1 highlighted in green. Frameshift site highlighted in blue. B) Phylogenetic analysis of mycovirus Rdp1 sequences. Scale bar represents the number of substitutions per site. Blue boxes on protein diagrams represent the reverse transcriptase (RT) domain of the Rdp1 protein. C) Protein sequence of the small dsRNA segment. The signal peptide is underlined and hydrophobic residues indicated with stars. D) Pictorial representation of predicted domains of the small dsRNA segment.

Figure 3. RNA-seq reveals transcriptional rewiring in virus-infected *M. sympodialis* strain. A) Dot plot of $\log_2$ fold-changes in gene expression in virus-infected strain. Red and blue dots represent upregulated and downregulated genes that pass a false discovery rate (FDR) of 5%, respectively. Gray dots are genes that do not meet the FDR. B) Number of genes upregulated (red) and downregulated (blue) categorized by gene ontology. C) Heat map of the three RNA-seq technical replicates of virus-infected and virus-cured strains. Green represents upregulated genes and red represents downregulated genes. D) Gene network map of upregulated genes in virus-infected strain. Genes are clustered by color based on the Markov-Cluster (MCL) inflation parameter.

Figure 4. Virus-infected strains cause enhanced inflammation in a murine ear skin infection model. A) Ear thickening, B) fungal load, and C) cytokine expression in the skin of mice that were epicutaneously infected with the indicated virus-infected and virus-cured strains for 4 days. Each symbol represents one mouse. In A), each value represents the mean of the ear thickness from both ears of each animal. The mean + SEM of each group is indicated. DL, detection limit. Statistics were calculated using One-way ANOVA. *p<0.05, ****p<0.0001. Black bars below the x-axis labels group virus-infected/virus-cured strain pairs. '+' indicates virus-infected, '-' indicates virus-cured.

Figure 5. MsMV1 dsRNA virus induces interferon-β (IFN-β) expression in cultured macrophages in a TLR3-independent manner. A) IFN-β expression in bone marrow-derived macrophages (BMDM) after infection with the indicated virus-infected and virus-cured strains at MOI=5 for 24 hours. Bars are the mean + SEM of four replicate samples with each being the pool of two separate wells. Data are pooled from two independent experiments. B) IFN-β expression by wildtype (solid bars) and *Tlr3*-/- (dashed bars) BMDM after infection with the indicated virus-infected and virus-cured strains at MOI=5 for 24 h. Bars are a pool of two wells. Data are representative of one out of two independent experiments. polyI:C (pI:C) was included as a positive control; US, unstimulated. The dotted line indicates the expression levels under unstimulated conditions. Statistics were calculated using unpaired Student's t test. *p<0.05, **p<0.01. Black bars below the x-axis labels group virus-infected/virus-cured strain pairs. '+' indicates virus-infected, '-' indicates virus-cured.

Supplemental Figure 1. *Malassezia* species harbor dsRNA segments. dsRNA from select *M. sympodialis* (A) and *M. furfur* (B) strains was analyzed by electrophoresis on a 0.8% agarose gel with 0.5 µg/mL ethidium bromide.

Supplemental Figure 2. Read coverage of the *M. sympodialis* strains KS012 and virus-cured SEC494 compared to the haploid reference strain ATCC42132.

Supplemental Figure 3. IL-17A and IFN-β expression in the *Malassezia*-infected ear skin is not altered by virus infection of the fungus. Cytokine transcripts were analyzed by RT-qPCR in the skin tissue of mice that were infected with the indicated strains for 2 days (A) or 7 days (B). Data are the mean + SEM from three mice per group. DL, detection limit. Statistics were calculated using One-way ANOVA. ****$p<0.0001$. Black bars below the x-axis labels group virus-infected/virus-cured strain pairs. '+' indicates virus-infected, '-' indicates virus-cured.

Supplemental Figure 4. Macrophage viability, CD86 expression, and TNF expression is not affected by the presence of MsMV1 in *M. sympodialis* strains. A) BMDM were infected with the indicated virus-infected and virus-cured strains at MOI=1 and analyzed for viability and CD86 surface expression by flow cytometry at 16 hours post-infection or infected at MOI=5 and analyzed for TNF expression by RT-qPCR at 24 hours post-infection. Each bar represents the mean + SEM of four samples, each being the pool of two separate wells. Data are pooled from two independent experiments. The dotted line indicates the expression levels under unstimulated conditions. B) Flow cytometry gating strategy used to assess BMDM viability (top row) and CD86 expression (bottom row). C) BMDM viability, CD86 surface expression and TNF expression of wild-type and *Tlr3*-/- BMDM infected with the indicated virus-infected and virus-cured strains and analyzed as in A). Data are from one out of two representative experiment with each value being the pool of two wells. Statistics were calculated using an unpaired Student's t test. *$p<0.05$. '+' superscripts indicate virus-infected strains, '-' superscripts indicate virus-cured.

Table 1. Strains used in dsRNA gel images. Strains are listed top to bottom in order of gel wells from left to right. If known, clinical data and sample location are listed. U = unknown, H =

healthy individual, D = dandruff, TV = tinea versicolor, PV = pityriasis versicolor, SD = seborrheic dermatitis, OE = otitis externa. '*' indicates strains sampled from an animal.

Table 2. Strains used in this study.

Table S1. Variants present only in the *M. sympodialis* virus-cured SEC494 compared to the virus-infected KS012.

File S1. Identification of the large dsRNA segment of the *M. sympodialis* MsMV1. Note that the designations "TRINITY_DN8321_c1_g1_i1 len=4613 path=[4591:0-4612] [-1, 4591, -2]" and "TRINITY_DN4986_c1_g1_i1 len=4601 path=[4579:0-4600] [-1, 4579, -2]" are automatically generated by the software Trinity. We arbitrary used the denomination DN8321 and DN4986 to indicate the contigs that represent the *M. sympodialis* MsMV1 mycovirus genome, as identified by blast analyses. Considering "TRINITY_DN8321_c1_g1_i1 len=4613 path=[4591:0-4612] [-1, 4591, -2]", according to the software instructions, TRINITY_DN8321_c1_g1_i1 indicates Trinity read cluster 'TRINITY_DN8321_c1', gene 'g1', and isoform 'i1'. 'Len' indicates the length of the cluster (contig) in bp, and path information indicates the path traversed in the Trinity compacted de Bruijn graph to construct that transcript.

File S2. Identification of the small dsRNA segment of the *M. sympodialis* MsMV1. For the contigs designation, see explanation in the legend of File S1.

File S3. Screenshot of the variants presents in the coding regions of the genes *KAE1* and *CRM1* in the *M. sympodialis* strains SEC494.

Figure 1

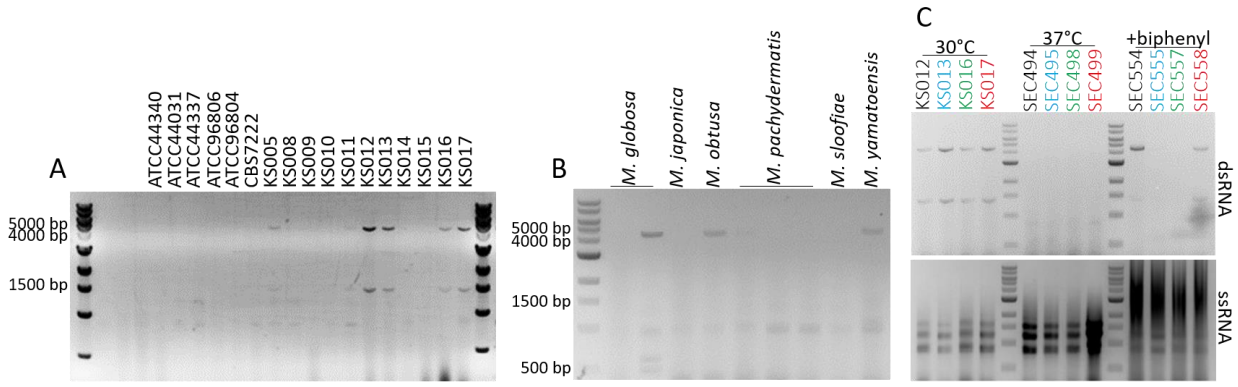
A
ATCC44340
ATCC44031
ATCC44337
ATCC96806
ATCC96804
CBS7222
KS005
KS008
KS009
KS010
KS011
KS012
KS013
KS014
KS015
KS016
KS017
5000 bp
4000 bp
1500 bp
B
M. globosa
M. japonica
M. obtusa
M. pachydermatis
M. slooffiae
M. yamatoensis
5000 bp
4000 bp
1500 bp
500 bp
C
30°C
37°C
+biphenyl
KS012
KS013
KS016
KS017
SEC494
SEC495
SEC498
SEC499
SEC554
SEC555
SEC557
SEC558
dsRNA
ssRNA

Figure 2

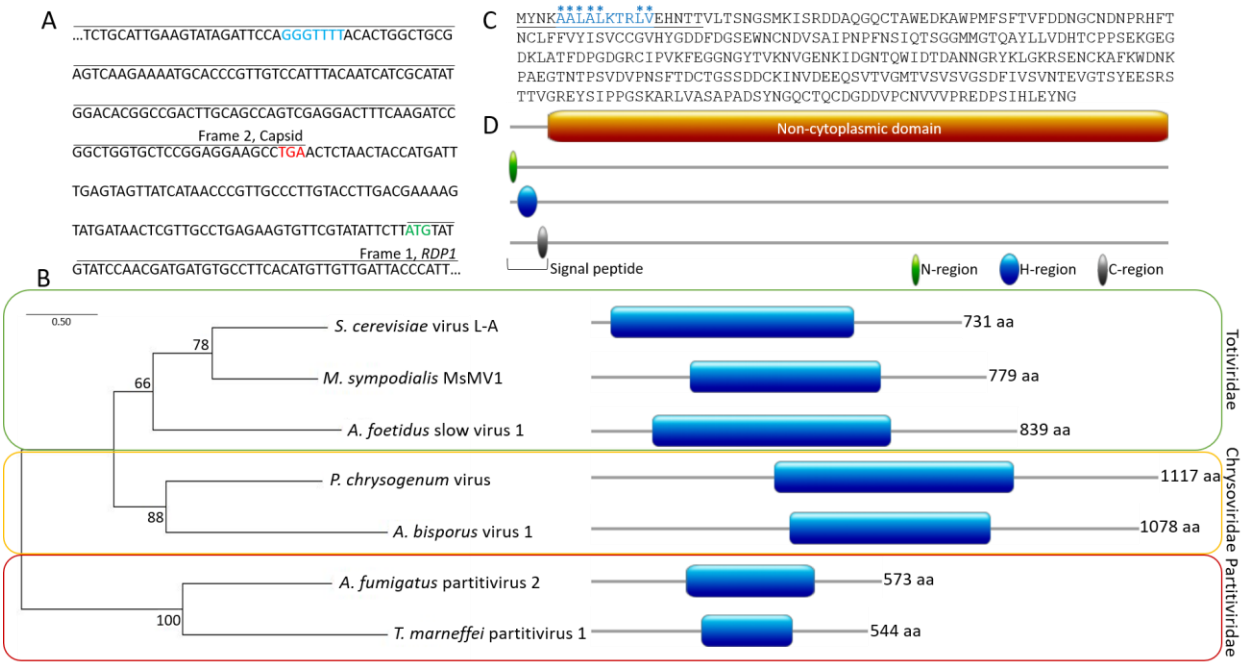
A
...TCTGCATTGAAGTATAGATTCCAGGGTTTTACACTGGCTGCG
AGTCAAGAAAATGCACCCGTTGTCCATTTACAATCATCGCATAT
GGACACGGCCGACTTGCAGCCAGTCGAGGACTTTCAAGATCC
Frame 2, Capsid
GGCTGGTGCTCCGGAGGAAGCCTGAACTCTAACTACCATGATT
TGAGTAGTTATCATAACCCGTTGCCCTTGTACCTTGACGAAAAG
TATGATAACTCGTTGCCTGAGAAGTGTTCGTATATTCTTATGTAT
Frame 1, RDP1
GTATCCAACGATGATGTGCCTTCACATGTTGTTGATTACCCATT...
C
MYNKAALALKTRLVEHNTTVLTSNGSMKISRDDAQGQCTAWEDKAWPMFSFTVFDDNGCNDNPRHFT
NCLFFVYISVCCGVHYGDDFDGSEWNCNDVSAIPNPFNSIQTSGGMMGTQAYLLVDHTCPPSEKGEG
DKLATFDPGDGRCIPVKFEGGNGYTVKNVGENKIDGNTQWIDTDANNGRYKLGKRSENCKAFKWDNK
PAEGTNTPSVDVPNSFTDCTGSSDDCKINVDEEQSVTVGMTVSVSVGSDFIVSVNTEVGTSYEESRS
TTVGREYSIPPGSKARLVASAPADSYNGQCTQCDGDDVPCNVVVPREDPSIHLEYNG
D
Non-cytoplasmic domain
Signal peptide
N-region
H-region
C-region
B
0.50
S. cerevisiae virus L-A
M. sympodialis MsMV1
A. foetidus slow virus 1
P. chrysogenum virus
A. bisporus virus 1
A. fumigatus partitivirus 2
T. marneffei partitivirus 1
78
66
88
100
731 aa
779 aa
839 aa
1117 aa
1078 aa
573 aa
544 aa
Totiviridae
Chrysoviridae
Partitiviridae

Figure 3

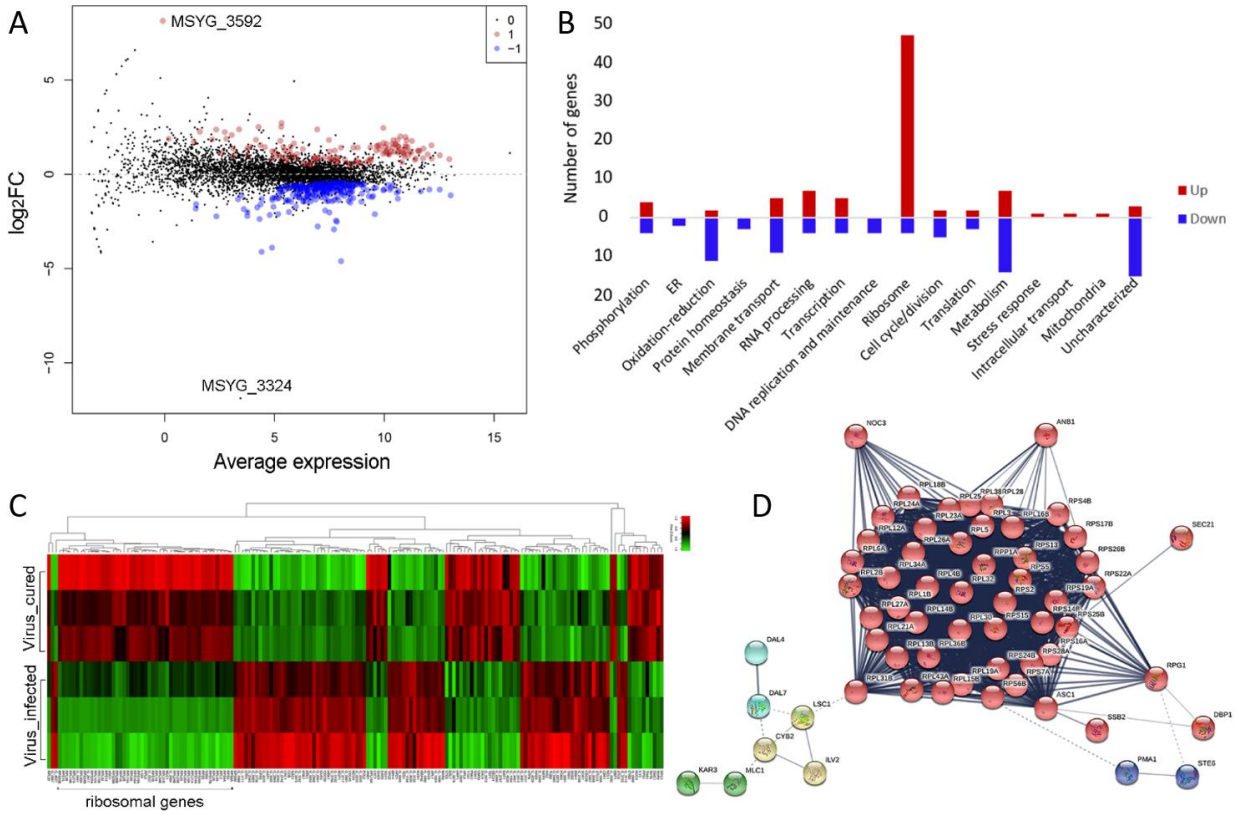
A
MSYG_3592
MSYG_3324
log2FC
Average expression
B
Number of genes
Up
Down
Phosphorylation
ER
Oxidation-reduction
Protein homeostasis
Membrane transport
RNA processing
Transcription
DNA replication and maintenance
Ribosome
Cell cycle/division
Translation
Metabolism
Stress response
Intracellular transport
Mitochondria
Uncharacterized
C
Virus_cured
Virus_infected
ribosomal genes
D

Figure 4

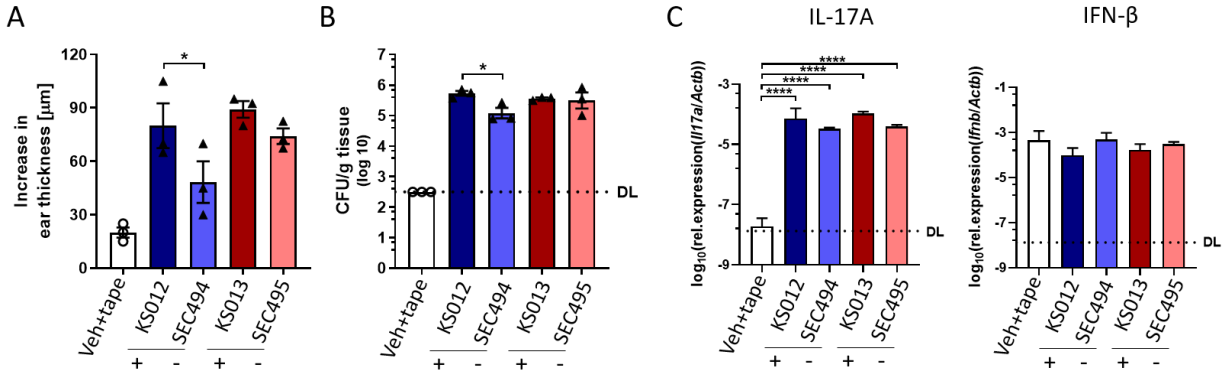
A
B
C
IL-17A
IFN-β
Increase in ear thickness [µm]
CFU/g tissue (log 10)
log10(rel.expression(Il17a/Actb))
log10(rel.expression(Ifnb/Actb))
DL
Veh+tape
KS012
SEC494
KS013
SEC495
+
-
*
****

Figure 5

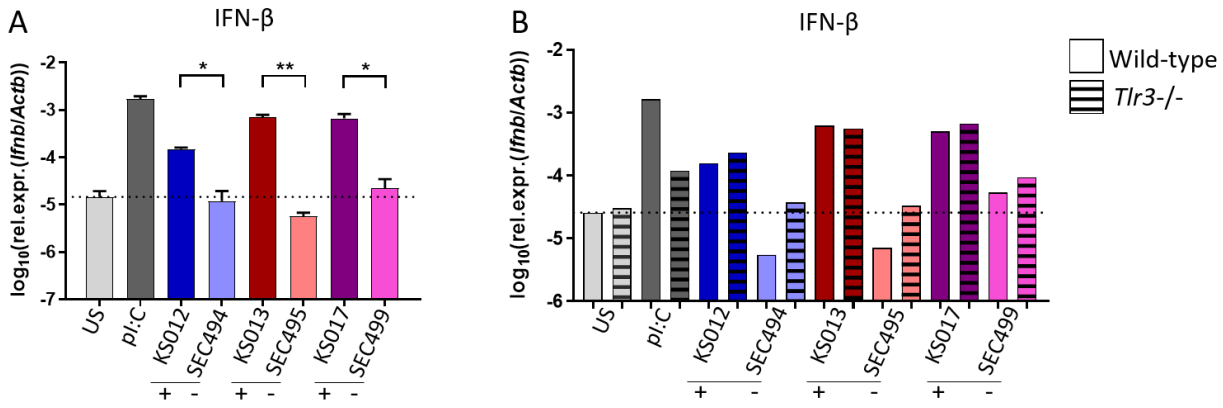
A
IFN-β
log10(rel.expr.(Ifnb/Actb))
-2
-3
-4
-5
-6
-7
*
**
*
US
pI:C
KS012
SEC494
KS013
SEC495
KS017
SEC499
+ -
+ -
+ -
B
IFN-β
log10(rel.expr.(Ifnb/Actb))
-2
-3
-4
-5
-6
Wild-type
Tlr3-/-
US
pI:C
KS012
SEC494
KS013
SEC495
KS017
SEC499
+ -
+ -
+ -

Figure S1

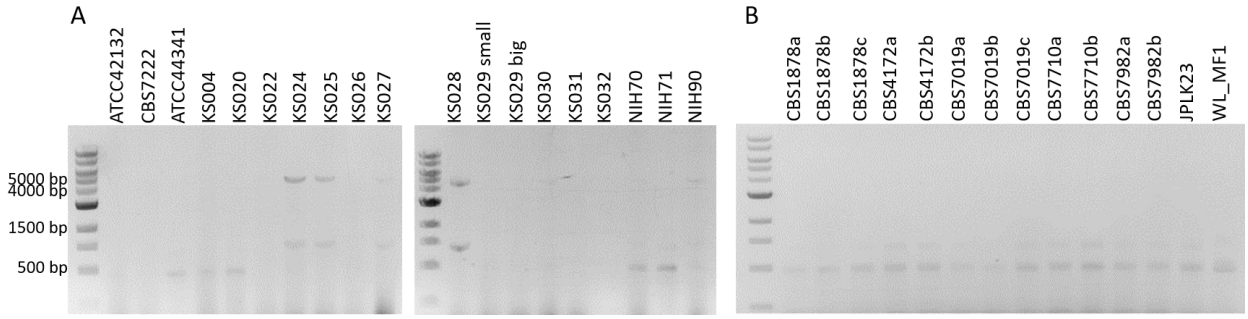
A
ATCC42132
CBS7222
ATCC44341
KS004
KS020
KS022
KS024
KS025
KS026
KS027
KS028
KS029 small
KS029 big
KS030
KS031
KS032
NIH70
NIH71
NIH90
5000 bp
4000 bp
1500 bp
500 bp
B
CBS1878a
CBS1878b
CBS1878c
CBS4172a
CBS4172b
CBS7019a
CBS7019b
CBS7019c
CBS7710a
CBS7710b
CBS7982a
CBS7982b
JPLK23
WL_MF1

Figure S2

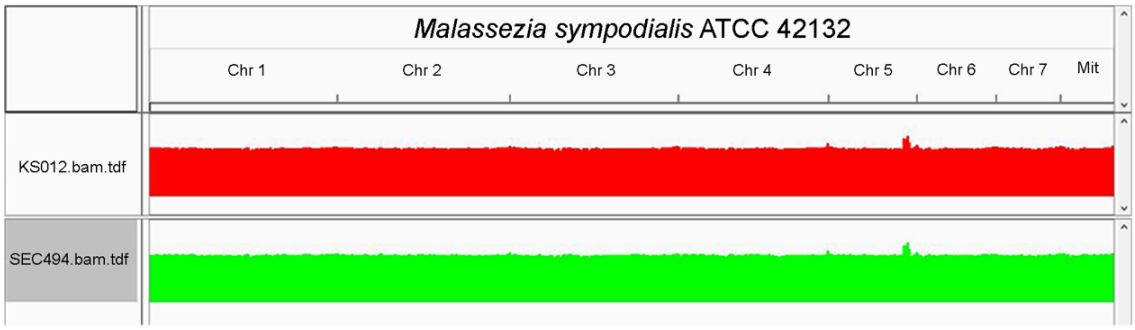
Malassezia sympodialis ATCC 42132
Chr 1
Chr 2
Chr 3
Chr 4
Chr 5
Chr 6
Chr 7
Mit
KS012.bam.tdf
SEC494.bam.tdf

Figure S3

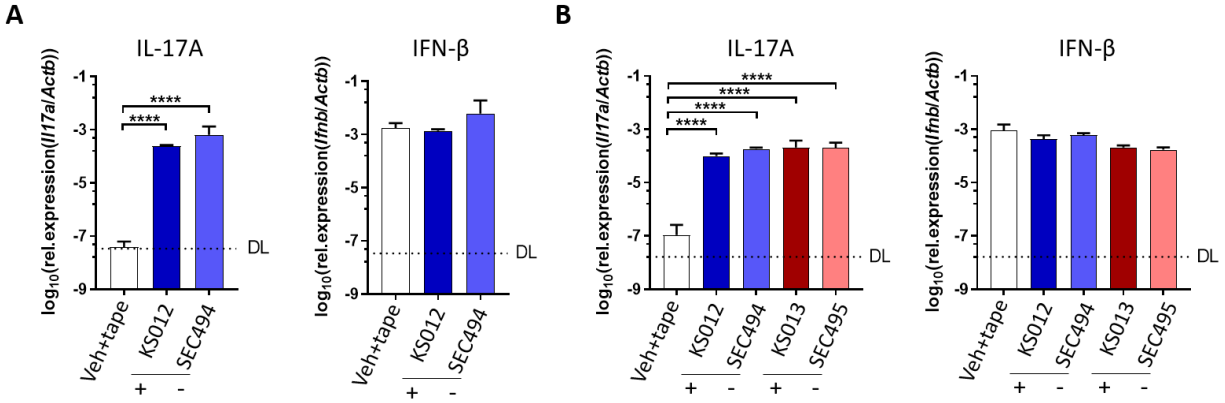
A
IL-17A
IFN-β
log10(rel.expression(Il17a/Actb))
log10(rel.expression(Ifnb/Actb))
-1
-3
-5
-7
-9
****
DL
Veh+tape
KS012
SEC494
+
-
B
IL-17A
IFN-β
KS013
SEC495

Figure S4

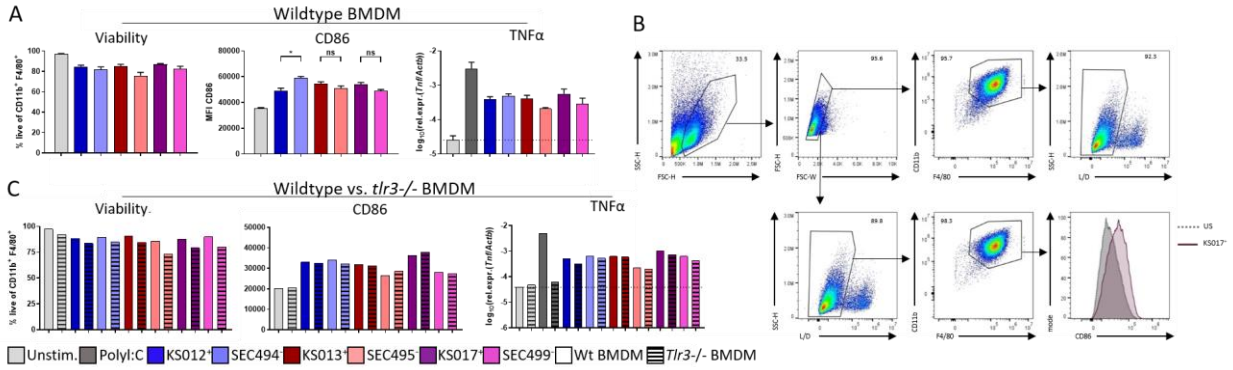
A
Wildtype BMDM
Viability
CD86
TNFα
B
C
Wildtype vs. tlr3-/- BMDM
Viability
CD86
TNFα
Unstim.
Polyl:C
KS012+
SEC494+
KS013+
SEC495+
KS017+
SEC499+
Wt BMDM
Tlr3-/- BMDM

1155 Table 1

Species	Strain	dsRNA	Fragment size(s)	Clinical data
M. sympodialis	ATCC44340	N	-	U
	ATCC44031	N	-	TV
	ATCC44337	N	-	U
	ATCC96806	N	-	H
	ATCC96804	N	-	TV
	CBS7222	N	-	U, ear
	KS005	Y	1500 bp, 4500 bp	H
	KS008	N	-	H
	KS009	N	-	H
	KS010	N	-	H
	KS011	N	-	H
	KS012	Y	1500 bp, 4500 bp	H
	KS013	Y	1500 bp, 4500 bp	H
	KS014	N	-	H
	KS015	N	-	H
	KS016	Y	1500 bp, 4500 bp	H
	KS017	Y	1500 bp, 4500 bp	H
	ATCC42132	N	-	TV
	ATCC44341	N	-	H
	KS004	N	-	H
	KS020	N	-	H
	KS022	N	-	H
	KS024	Y	1500 bp, 4500 bp	H
	KS025	Y	1500 bp, 4500 bp	H
	KS026	N	-	H
	KS027	N	1500 bp, 4500 bp	H
	KS028	Y	1300 bp, 4500 bp	H
	KS029small	N	-	H
	KS029big	N	-	H
	KS030	N	-	H
	KS031	N	-	H
	KS032	N	-	H
	NIH70	N	-	H
	NIH71	N	-	H
	NIH90	Y	4500 bp	H
M. furfur	CBS1878a	N	-	D, scalp
	CBS1878b	N	-	D, scalp
	CBS1878c	N	-	D, scalp
	CBS4172a	N	-	U
	CBS4172b	N	-	U
	CBS7019a	N	-	PV, torso
	CBS7019b	N	-	PV, torso
	CBS7019c	N	-	PV, torso

	CBS7710a	N	-	U
	CBS7710b	N	-	U
	CBS7982a	N	-	H, ear
	CBS7982b	N	-	H, ear
	JPLK23	N	-	U, blood
	WL_MF1	N	-	U, scalp
M. globosa	CBS7866	N	-	U
	CBS7874	Y	500 bp, 600 bp, 4500 bp	D, scalp
M. japonica	CBS9431	N	-	H
M. obtusa	CBS7876	Y	4500 bp	U
M. pachydermatis	DUMC184.03	Y	4500 bp	U*, ear
	CBS1879a	N	-	OE*, ear
	CBS1879b	N	-	OE*, ear
M. sloofiae	CBS7956	N	-	H*, ear
M. yamatoensis	CBS9725	Y	4500 bp	SD

U = unknown, H = healthy individual, D = dandruff, TV = tinea versicolor, PV = pityriasis versicolor, SD = seborrheic dermatitis, OE = otitis externa.

'*' indicates strains sampled from an animal.

1156

1157

1158

1159

1160

1161

1162

1163

1164

1165

1166

1167

1168

1169

1170

1171

Table 2

Strain name	Details
KS012	*M. sympodialis*; MsMV1-infected
KS013	*M. sympodialis*; MsMV1-infected
KS016	*M. sympodialis*; MsMV1-infected
KS017	*M. sympodialis*; MsMV1-infected
SEC494	*M. sympodialis*; MsMV1 temperature-cured congenic strain of KS012
SEC495	*M. sympodialis*; MsMV1 temperature-cured congenic strain of KS013
SEC498	*M. sympodialis*; MsMV1 temperature-cured congenic strain of KS016
SEC499	*M. sympodialis*; MsMV1 temperature-cured congenic strain of KS017
SEC554	*M. sympodialis*; MsMV1 biphenyl-passaged congenic strain of KS012
SEC555	*M. sympodialis*; MsMV1 biphenyl-cured congenic strain of KS013
SEC557	*M. sympodialis*; MsMV1 biphenyl-cured congenic strain of KS016
SEC558	*M. sympodialis*; MsMV1 biphenyl-passaged congenic strain of KS017

Table S1

cation	ele	nsequence	pact	ne	mbol	scription	cession
671822.1:1098983-1098983		ssense_variant	derate	SYG_1556	*E1*	ghly conserved ATPase of HSP70/DnaK family	O77215
671824.1:502360-502360		ssense_variant	derate	SYG_1556	*M1*	jor karyopherin	O78388